

First-Principles Assessment of the Reactions of Boric Acid on NiO(001) and ZrO₂($\bar{1}11$) Surfaces

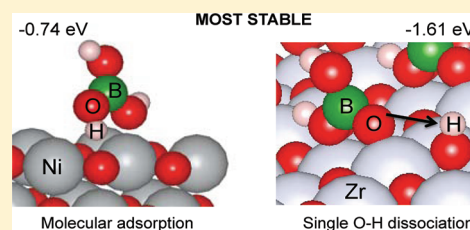
Priyank V. Kumar,[†] Michael P. Short,[‡] Sidney Yip,[‡] Bilge Yildiz,^{*,‡} and Jeffrey C. Grossman^{*,†}

[†]Department of Materials Science and Engineering, Massachusetts Institute of Technology, Cambridge, Massachusetts, United States

[‡]Department of Nuclear Science and Engineering, Massachusetts Institute of Technology, Cambridge, Massachusetts, United States

S Supporting Information

ABSTRACT: The present study investigates the adsorption and dissociation reaction pathways of boric acid, B(OH)₃, and the reaction kinetic descriptors on NiO(001) and ZrO₂($\bar{1}11$) surfaces. Density functional theory is employed for ground-state calculations, while the nudged elastic band method is used for obtaining reaction barriers. Strong electron correlations in the case of NiO are included using the DFT + *U* approach. Adsorption of boric acid on clean ZrO₂($\bar{1}11$) is found to be more favorable compared with that on NiO(001), in agreement with prior experiments. Dissociative adsorption is observed to dominate over molecular adsorption in the case of ZrO₂($\bar{1}11$), whereas NiO(001) favors molecular adsorption. The most stable configuration for B(OH)₃ on NiO(001) is a hydrogen-bonded molecular structure, Ni_s-(OH)B(OH)(OH)⋯O_s (s = surface atom), with an adsorption energy of −0.74 eV. On ZrO₂($\bar{1}11$), a single O–H dissociated structure, Zr_s-(O)B(OH)(HO)-Zr_s + O_s-H, with an adsorption energy of −1.61 eV, is the most stable. Our results reveal lower activation barriers for B(OH)₃ dissociation on NiO(001) than on ZrO₂($\bar{1}11$). We demonstrate the importance of both the surface transition-metal atom and oxygen states and discuss bonding mechanisms leading to different adsorption configurations on such metal oxides. The analysis of surface reactivity presented here is useful in designing metal oxides for catalytic applications and is of significant importance in fuel materials durability in nuclear energy systems.



INTRODUCTION

Transition-metal oxide (TMO) surfaces have been of significant importance for a wide range of applications, including catalysis,^{1,2} thin-film coatings,³ fuel cells,^{4–6} and gas sensors.⁷ In such applications, a critical understanding of the surface reactivity and adsorption/dissociation reactions in various environments becomes necessary. In addition, understanding and control of surface reaction kinetics is of significant relevance in the field of corrosion and chemical sensors.

Adsorption of boric acid on TMOs has been of interest for a broad range of reasons in the past. For example, boric acid adsorption on TiO₂ has been studied in the context of dye-sensitized solar cells,^{8,9} to convert sunlight into electricity. Boric acid incorporation in soils has been investigated as boron is an important micronutrient for plants.¹⁰ In the present work, our focus is on understanding the process of boron poisoning in nuclear reactors that leads to the safety issue of unequal axial power distribution along the fuel rods.¹¹ The accumulation and incorporation of boron inside the corrosion deposits (namely, the CRUD) on the nuclear fuel cladding is believed to play a major role in neutron flux depression. The source of boron is the boric acid that is added to control the neutron activity in nuclear reactors. Previous work^{11–15} reveals that boron incorporation and deposition into the corrosion deposits could occur by adsorption and solid-state reactions or precipitation from water. In particular, experiments¹⁴ on CRUD oxides report the following trend for the adsorption strength of boron among the substrates: Fe₃O₄ > NiFe₂O₄ >

ZrO₂ > NiO. It is suggested that the adsorbing boron species is likely to be the neutral boric acid molecule and that the formation of surface complexes on CRUD oxides could lead to precipitation of boron containing compounds, such as the bonaccordite (Ni₂FeBO₅). Although these experiments report the collective adsorption behavior on CRUD oxides, an atomic scale mechanistic description of boric acid adsorption and dissociation is still lacking. Rate-theory modeling at the continuum level has helped to explain certain aspects of heat, momentum, and mass transfer with respect to CRUD deposition in general.^{16,17} However, in order to predict the kinetics of such mechanisms, the present study aims to describe the surface reaction mechanisms of boric acid on relevant oxides at the atomic level using first-principles quantum mechanical calculations. We choose NiO and ZrO₂ substrates as the model systems in this work.

Bulk ZrO₂ exhibits several polymorphs for different ranges of temperature and pressure. However, studies have shown that ZrO₂ deposits found in CRUD have a monoclinic structure.¹⁸ Hence, we study adsorption characteristics on the monoclinic ZrO₂ phase. On the other hand, we choose to study NiO in its usual rocksalt structure and antiferromagnetic state. Reactor environments are complex in terms of the chemistry of solid materials as well as of water. The oxide surfaces are

Received: February 17, 2012

Revised: April 16, 2012

Published: May 1, 2012

hydroxylated in an aqueous environment, and the degree of hydroxylation can vary depending on the coolant chemistry and operating temperature. In addition to the hydroxyl species, surface defects, such as oxygen vacancies, are likely to exist. Such complexities could, in general, lead to a competition among different surface terminations and reconstructions in terms of stability. In the case of NiO, temperature dependence in the development of low-energy electron diffraction (LEED) patterns associated with the NiO surface has shown that NiO(111) surfaces become unstable above 300 K and that the NiO(001) and metallic Ni(001) develop at the expense of a 7×7 -like structure¹⁹ above 500 K. Other experiments reveal the presence of a bicrystalline NiO(001) and NiO(111) surface structure.^{20,21} On oxidation at 500 K, it is shown that the NiO(001) regions dominate with around 93% surface coverage, and on exposure to water, this can decrease to 75–91%, with NiO(001) regions still being dominant.²¹ Thus, using surface models with NiO(001) is reasonable. Furthermore, patches of NiO(111), if present, are strongly hydroxylated and are proposed to be passive. On the other hand, NiO(001) regions are not hydroxylated except at the defect sites.^{20,21} In the case of monoclinic ZrO₂, the ($\bar{1}11$) surface is the most stable even under the hydroxylated condition.^{22,23} The water desorption temperature for the ($\bar{1}11$) surface is reported to be about 633 K, although the presence of hydroxyl groups on other planes is still observed.²⁴

With this background and as a first step toward developing a capability to understand and predict boron incorporation mechanisms and kinetics into CRUD oxides, we choose to work with NiO(001) and monoclinic ZrO₂($\bar{1}11$) surfaces, in their defect-free and nonhydroxylated states. We use density functional theory (DFT) calculations to study molecular and dissociative adsorption of boric acid on these surfaces. The nudged elastic band (NEB) method is employed to determine the reaction barriers. On the basis of the energetics, we explain the trends in surface affinity of NiO and ZrO₂ toward boric acid. We demonstrate that, taken together, such computational studies can help us understand boron deposition mechanisms, predict oxides that can significantly repel boron, provide crucial guidance to better control coolant chemistry, and design novel nuclear fuel rod materials to prevent boron deposition.

COMPUTATIONAL METHOD

All calculations in this work have been performed using DFT as implemented in the Vienna Ab-initio Simulation Package (VASP).²⁵ NiO is an example of a strongly correlated system experiencing an on-site Coulombic repulsion that is not correctly described by DFT alone.²⁶ Hence, for NiO, the DFT + *U* scheme of Dudarev et al.²⁷ has been implemented with *U* = 6.3 eV and *J* = 1 eV.²⁶ The projector augmented wave (PAW) method^{28,29} is used for electron–ion interaction in the case of NiO, whereas the ultrasoft pseudopotentials are used for ZrO₂. The generalized gradient approximation (GGA) in the form of the Perdew–Wang functional (PW91) is used.³⁰ Spin-polarized calculations are performed only for NiO using the Vosko et al. interpolation scheme.³¹ A Gaussian smearing approach with σ = 0.2 eV has been used for NiO, whereas the tetrahedron method with Blochl corrections^{32,33} is used for ZrO₂. The plane-wave energy cutoff is fixed at 600 eV for NiO and 500 eV for ZrO₂. For the slab calculations, a vacuum region greater than 10 Å is maintained and a Monkhorst–Pack $3 \times 3 \times 1$ grid³⁴ is used for *k*-point sampling. In all simulations, the

ions are relaxed until the Hellman–Feynman forces on each atom are smaller than 0.03 eV/atom.

We use a well-converged five-layer slab for the NiO(001) surface and a four-layer slab for the ZrO₂($\bar{1}11$) surface, as shown in Figure 1a. The construction of the two-dimensional

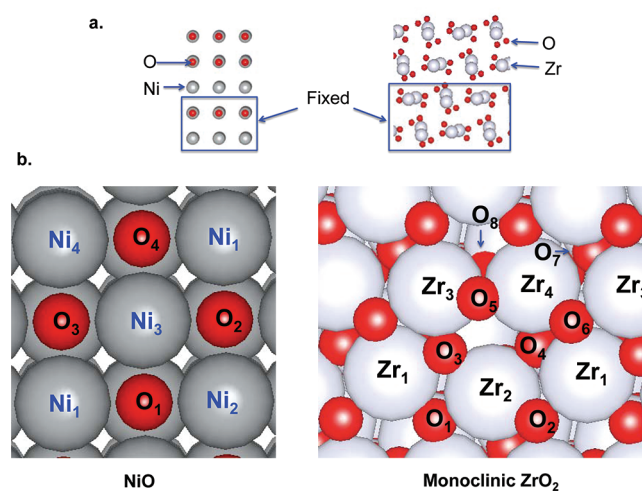


Figure 1. (a) Slab models used for NiO(001) and monoclinic ZrO₂($\bar{1}11$) surfaces. (b) Top view of the NiO(001) and monoclinic ZrO₂($\bar{1}11$) surfaces. The NiO surface unit cell chosen consists of four Ni and O atoms, while the ZrO₂ surface unit cell consists of four Zr and eight O atoms. The numbering scheme is used to characterize adsorption structures later.

surface unit cell for ZrO₂($\bar{1}11$) is described elsewhere.²⁴ The two-dimensional surface unit cell is chosen such that it contains four Ni and O atoms (or four Zr and eight O atoms), as shown in Figure 1b. In the case of NiO, the top three layers are allowed to relax, while keeping the bottom two layers fixed to simulate bulk. For the ZrO₂ case, the top three layers are allowed to relax while keeping the bottom layer fixed. We perform adsorption studies for a surface coverage of 25%, which we define as one boric acid molecule per four surface Ni (or Zr) atoms. The numbering scheme on the atoms will be used to index them in the adsorption structures discussed later. The structural and electronic properties of bulk NiO and monoclinic ZrO₂ using the methodology described above are presented in Tables S1 and S2 (Supporting Information), and they show good agreement with previous calculations and experiments (see the Supporting Information).

The adsorption energy is calculated using the expression

$$E_{\text{ads}} = E_{(\text{slab}+\text{molecule})} - E_{\text{slab}} - E_{\text{molecule}} \quad (1)$$

where E_{slab} represents the energy of a clean slab, E_{molecule} represents the energy of the adsorbate in the gas phase, and $E_{(\text{slab}+\text{molecule})}$ represents the total energy after adsorption. A negative adsorption energy indicates exothermicity and favorable adsorption. We use the NEB method for calculating reaction barriers as implemented in VASP. Typically, 9–13 images were used in between the reactant and the product structures, to obtain well-converged reaction pathways and activation barriers. The force criterion for convergence was kept at 0.03 eV/atom.

RESULTS AND DISCUSSION

Pristine NiO(001) and ZrO₂($\bar{1}11$) Surfaces. Prior to studying adsorption and surface reactions, we identified the

most stable surface terminations in our simulations and their properties. The (001) surface of NiO is found to be the most stable termination. It is nonpolar, with a surface energy of 0.88 J/m^2 (55 meV/\AA^2). The magnetic moment of the surface Ni atom is $1.69 \mu_B$. These results are in good agreement with the surface energy value of 49 meV/\AA^2 and a magnetic moment value of $1.71 \mu_B$, as obtained by Rohrbach et al.²⁶ The surface also exhibits an antiferromagnetic state. In the case of ZrO_2 , the (111) surface is the most stable with a surface energy of 1.215 J m^{-2} , in good agreement with the value of 1.246 J m^{-2} obtained by Christensen and Carter.³⁵

Structure of B(OH)_3 . The boric acid molecule exists in two forms, cis and trans conformations, in the gas phase. The trans conformation is found to be more stable by 0.17 eV , in good agreement with the theoretical value of 0.18 eV obtained by Raghunath and Lin.⁸ The optimized structures are shown in Figure 2, and structural data are presented in Tables 1 and 2.

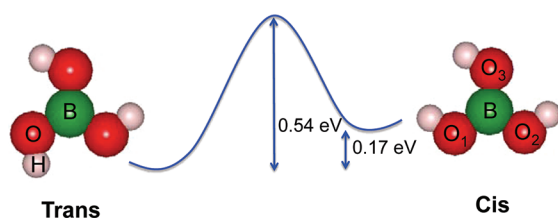


Figure 2. Structure and energetics of trans and cis conformers of boric acid.

Table 1. Structural Data of the *trans*- B(OH)_3 Molecule

	present work	calculated (B3LYP) ³⁶	experiment (crystalline) ³⁷
B–O (Å)	1.377	1.380	1.367
O–H (Å)	0.972	0.971	0.970
$\angle\text{OBO}$ (deg)	112.5	112.6	113.3

Table 2. Structural Data of the *cis*- B(OH)_3 Molecule

	present work	calculated ¹⁸
B–O ₁ (Å)	1.379	1.374
B–O ₂ (Å)	1.373	1.368
B–O ₃ (Å)	1.387	1.382
$\angle\text{O}_1\text{BO}_2$ (deg)	116.0	116.6
$\angle\text{O}_2\text{BO}_3$ (deg)	118.2	
$\angle\text{O}_3\text{BO}_1$ (deg)	125.8	

NEB calculations reveal that the trans configuration has to overcome an activation barrier of 0.54 eV to transform to the higher-energy cis state. In our study, we have accounted for several possible adsorption structures. Fundamentally, we expect two modes of adsorption: molecular and dissociative. However, one mode can dominate over the other depending on the adsorbate–adsorbent interactions. The adsorption structure can be monodentate or bidentate, depending on the number of atoms of B(OH)_3 bonded to the surface, and dissociation of one or two O–H bonds of the boric acid molecule can occur on the surface. In addition, H_2O elimination reactions are possible on these surfaces, and the stability of the dissociated structures formed depends on the adsorbent.

Adsorption Configurations of B(OH)_3 on NiO(001). Several possible modes of adsorption and adsorption configurations were studied for B(OH)_3 on NiO(001). The most favorable relaxed structures for molecular and dissociative

adsorption cases are presented in Figure 3. The most stable adsorption configuration of B(OH)_3 on NiO(001) is the

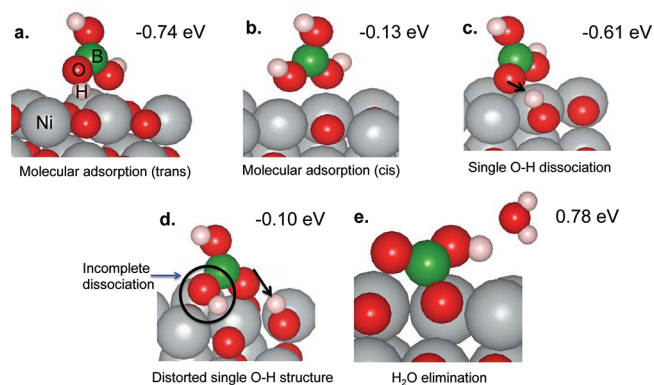


Figure 3. Reaction sequence showing the most favorable molecular and dissociated adsorption configurations of B(OH)_3 on NiO(001), and the corresponding adsorption energy values. Note that the double O–H bond dissociation is unstable, and we obtain a distorted single O–H dissociated structure. The arrows in black indicate dissociation.

molecular monodentate structure $\text{Ni}_3\text{-(OH)B(OH)(OH)}\cdots\text{O}_2$ (Figure 3a). In this structure, the O atom of a hydroxyl group is bonded to a surface Ni atom, while the H atom of another hydroxyl group forms a hydrogen bond with a surface O atom. The adsorption energy of this structure is -0.74 eV . All energies are referenced to the initial reactants, $\text{NiO(001)} + \text{trans-B(OH)}_3$. We also assessed the variation of adsorption energy with the tilting angle of the B(OH)_3 molecule on the surface. This result shows that tilting of B(OH)_3 does not require a large energy penalty ($<0.08 \text{ eV}$) and implies that, with rising temperatures, the boric acid molecule could explore several orientations on the surface (see the Supporting Information).

Another type of molecular adsorption configuration observed is with the cis form of B(OH)_3 , $\text{Ni}_2\text{-(OH)B(OH)(HO)-Ni}_3$, as shown in Figure 3b. This is a bidentate structure with a low adsorption energy of -0.13 eV . The dissociation of one of the hydroxyl groups on the surface is found to be metastable. This leads to a bidentate dissociated structure $\text{Ni}_2\text{-OB(OH)(OH)-Ni}_3 + \text{O}_2\text{-H}$ (Figure 3c), with an adsorption energy of -0.61 eV . The dissociation of two hydroxyl groups was found to be unstable. Although simulations started with double O–H configurations, upon relaxation, we could not observe any clear double O–H dissociated structures. Instead, we obtain a distorted single O–H dissociated structure with a low adsorption energy of -0.10 eV , as shown in Figure 3d. Dissociation reactions of B(OH)_3 to yield a water molecule were explored as well. We examined different adsorption configurations and found that, for the NiO(001) case, these reactions are endothermic and, thus, unfavorable. Figure 3e shows the structure that is least endothermic. In this bidentate structure, $\text{Ni}_2\text{-OB(O}_1\text{)O} + \text{H}_2\text{O}$, we observe that the B atom binds with one of the surface O atoms, in order to form three B–O bonds, eliminating a water molecule in the process. This structure is found to have an adsorption energy of 0.78 eV . In summary, these results highlight that the molecular monodentate structure and the bidentate single O–H dissociated structure are likely to form on the NiO(001) surface.

Adsorption Configurations of B(OH)_3 on $\text{ZrO}_2(111)$. As with the NiO(001) surface, we considered a number of

adsorption structures for $\text{B}(\text{OH})_3$ on $\text{ZrO}_2(\bar{1}11)$. There are five oxygen atoms exposed on the surface, which leads to a wide variety of possible adsorption configurations. First, we note that molecular adsorption is significantly favorable in both the hydrogen-bonded monodentate, $\text{Zr}_3\text{-(OH)B(OH)(OH)}\cdots\text{O}_5$ (Figure 4a), and the bidentate, $\text{Zr}_2\text{-(OH)B(OH)(HO)-Zr}_3$

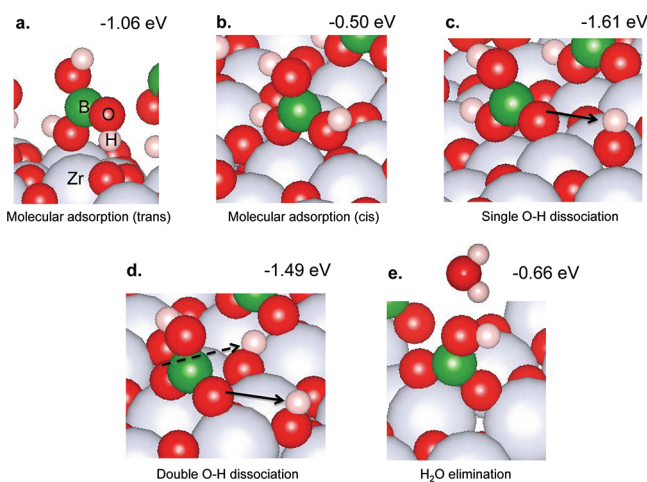


Figure 4. Reaction sequence showing the most favorable molecular and dissociated adsorption configurations of $\text{B}(\text{OH})_3$ on $\text{ZrO}_2(\bar{1}11)$, and the corresponding adsorption energy values. The arrows in black indicate dissociation.

(Figure 4b), configurations. The monodentate trans form is more stable with an adsorption energy of -1.06 eV, whereas the bidentate cis form has an adsorption energy of -0.50 eV. All the energy values are referenced to the initial reactants, the $\text{ZrO}_2(\bar{1}11) + \text{trans-B}(\text{OH})_3$ system. Our calculations suggest that dissociation of $\text{B}(\text{OH})_3$ is highly probable, resulting in the most stable single O–H dissociated bidentate structure, $\text{Zr}_2\text{-OB(OH)(HO)-Zr}_3 + \text{O}_5\text{-H}$ (Figure 4c), with an adsorption energy of -1.61 eV. Further dissociation of $\text{B}(\text{OH})_3$ is also observed to be favorable, unlike the NiO case. The double O–H dissociated bidentate structure $\text{Zr}_2\text{-OB(OH)O-Zr}_3 + \text{O}_5\text{-H} + \text{O}_6\text{-H}$ (Figure 4d) is found to have an adsorption energy of -1.49 eV. Water elimination reactions are found to be favorable on the $\text{ZrO}_2(\bar{1}11)$ surface. Several structures were tested in this regard. We found that one of these structures, $\text{Zr}_3\text{-OB(O}_5\text{)-(OH)} + \text{H}_2\text{O}$ (Figure 4), a bidentate with one of the O atoms bonded to a surface Zr atom and the B atom bonded to a surface O atom, is likely to form. The adsorption energy of this structure is found to be -0.66 eV. Additional adsorption configurations of $\text{B}(\text{OH})_3$ on ZrO_2 have been explored and reported (see the Supporting Information). In summary, these results indicate that $\text{B}(\text{OH})_3$ dissociatively adsorbs onto the $\text{ZrO}_2(\bar{1}11)$ surface and that the bidentate single and double O–H dissociated structures are most likely to be formed consequently.

Bonding Mechanism on the Basis of the Electronic Structure of the Surfaces. To explain our observations regarding molecular and dissociative adsorption of $\text{B}(\text{OH})_3$ on NiO(001) and $\text{ZrO}_2(\bar{1}11)$ surfaces, we turn our attention to the bonding mechanisms and the inherent electronic structure of the surfaces. The reactivity of an oxide surface that exposes both cations and anions can be explained using a simple Lewis acid–base picture. The cation sites act as Lewis acids attracting the oxygen atoms of the adsorbate, while the surface anion sites

(oxygen, in this case) act as Lewis bases attracting hydrogen atoms of the adsorbate. Thus, the strength of this Lewis acid–base pair determines the dissociation of the boric acid molecule.

The bonding mechanism of the $\text{B}(\text{OH})_3$ molecule with the transition-metal atom, in general, can be understood from the hybridization of the $\text{B}(\text{OH})_3$ molecule states with the d orbitals (t_{2g} and e_g states) of the metal atom in the relevant energy range. In this regard, the interaction of empty e_g states with $\text{B}(\text{OH})_3$ leads to adsorbate–adsorbent bonds, while the interaction of filled t_{2g} states contributes to the reduction of the intramolecular O–H bond strength of the boric acid molecule, favoring dissociation. Another factor that contributes to dissociation is the Lewis base strength of the surface O atom, which can be determined from the surface states of O atoms. Taking these two factors into account helps us to understand NiO(001) and $\text{ZrO}_2(\bar{1}11)$ surface reactivity toward $\text{B}(\text{OH})_3$.

The projected density of states (PDOS) before and after adsorption, taking into account the most stable molecular and dissociative adsorption configurations of $\text{B}(\text{OH})_3$ on NiO(001) and $\text{ZrO}_2(\bar{1}11)$, are given in Figures 5 and 6, respectively. In Figure 5a, showing the scenario of molecular adsorption on NiO(001), we note that the e_g orbitals of the surface Ni atoms interact with the lone pair on the O atom of the $\text{B}(\text{OH})_3$ molecule, forming the adsorbate–adsorbent bond. However, we see that the filled t_{2g} orbitals interact insignificantly in this molecular configuration. In Figure 5b, which concerns dissociative adsorption, the e_g orbitals of the surface Ni atom undergo strong interactions while the t_{2g} orbitals remain practically unperturbed, rendering the O–H bond dissociation difficult and thus destabilizing the dissociated structure. Hence, molecular adsorption is preferred with the NiO(001) surface. In the case of molecular adsorption of $\text{B}(\text{OH})_3$ on $\text{ZrO}_2(\bar{1}11)$, as shown in Figure 6a, we observe a similar trend as seen with NiO(001). In contrast to that on NiO(001), upon dissociative adsorption, as shown in Figure 6b, the t_{2g} orbitals interact strongly and are pushed downward in energy, favoring dissociative adsorption. As mentioned earlier, another factor determining dissociation of $\text{B}(\text{OH})_3$ is the surface O states. Clearly, the O states in the case of the clean $\text{ZrO}_2(\bar{1}11)$ surface (Figure 6) are more pronounced compared with the O states on clean NiO(001) (Figure 5). This shows that the Lewis acid strength of the exposed ZrO_2 oxygen atoms is higher, leading to a greater driving force for dissociative adsorption, which is consistent with our findings from DFT calculations of adsorption. These O states interact strongly with protons, upon dissociation of $\text{B}(\text{OH})_3$, as seen in Figures 5b and 6b. Such an understanding of the surface reactivity on the basis of surface PDOS can guide the design of metal oxide surface properties to our interest, for example, in designing metal oxide catalysts, or fuel rod surfaces that prevent corrosion product deposition and thus repel boron in nuclear reactors.

Energy Barriers in the Dissociation of $\text{B}(\text{OH})_3$ on NiO(001) and $\text{ZrO}_2(\bar{1}11)$. Assessment of the energy barriers for the dissociation of $\text{B}(\text{OH})_3$ provides kinetic descriptors of the initial phases of boron deposition on the selected surfaces. The potential energy diagram showing the reaction energy barriers following the adsorption of $\text{B}(\text{OH})_3$ on NiO(001) is given in Figure 7, starting with either a trans configuration (Path 1) or a cis configuration (Path 2) of the adsorbed molecule. Being most favorable, molecular adsorption of $\text{B}(\text{OH})_3$ on NiO(001) is the first step. Starting with *trans*- $\text{B}(\text{OH})_3$, the molecular monodentate form (I) can then dissociate into a bidentate single O–H dissociated structure

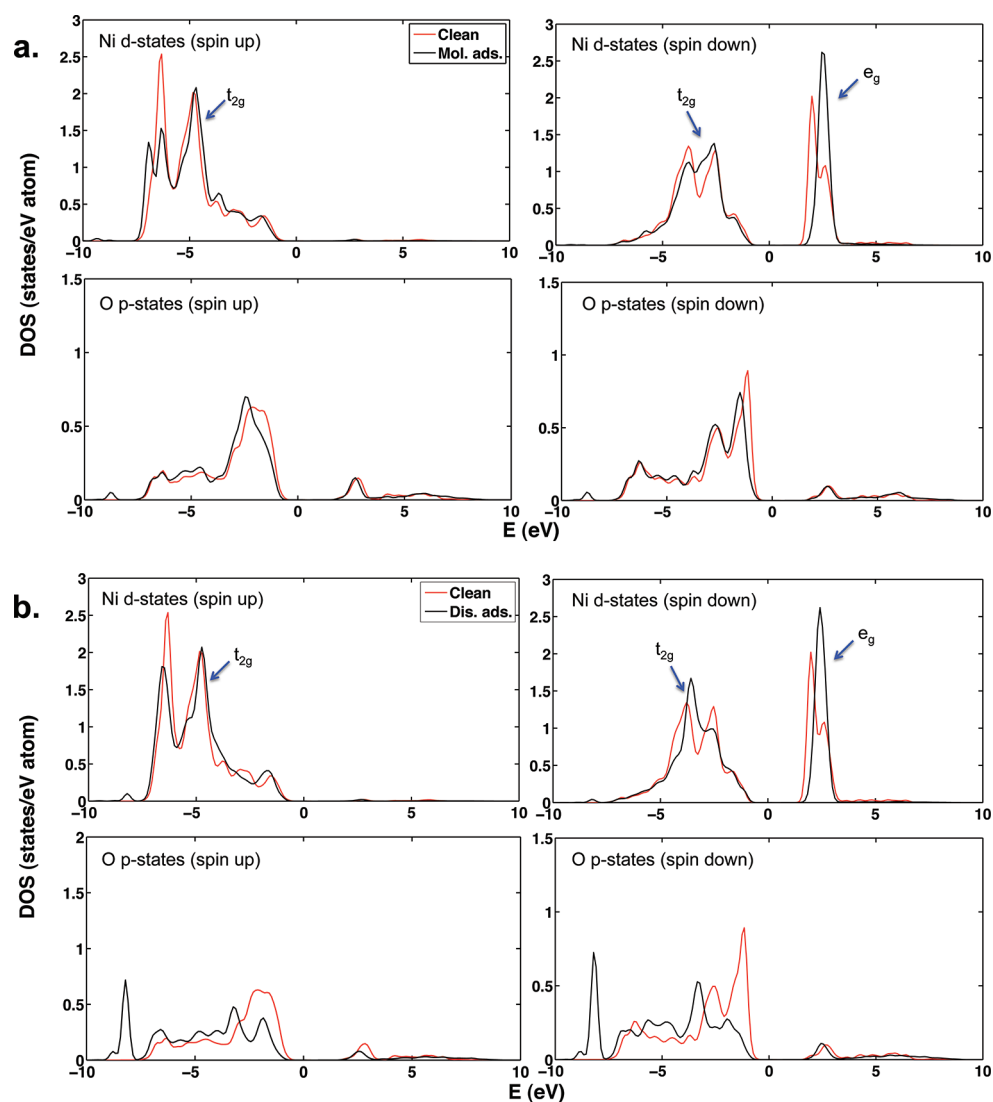


Figure 5. Projected density of states (PDOS) for the surface Ni and O atoms, obtained in the case of the most stable molecular adsorption (a) and dissociative adsorption (b). The states for the clean and adatom sites are marked in red and black, respectively.

(2), depicted as Path 1. The H atom of the $B(OH)_3$ molecule forming a hydrogen bond with a surface O atom dissociates and forms a hydroxyl group. The boric acid molecule rotates toward a Ni atom and forms a bidentate structure. The activation barrier for this forward reaction is predicted to be 0.15 eV, and the backward reaction is found to be practically barrierless with an activation barrier as low as 0.02 eV. Since the reaction rate varies as $\exp(-\Delta E_{act}/kT)$, assuming the pre-exponential factor to be a constant, these results suggest that the reaction rates are significantly higher even at moderate temperatures. An alternative path to the dissociation reaction starts from a *cis*- $B(OH)_3$ molecule and is also shown in Figure 7 (Path 2). In this case, the bidentate molecular structure (3) can also undergo single O–H dissociation where one of the H atoms close to the surface dissociates and binds with a surface O atom, resulting in the formation of a single O–H dissociated structure (2). The barrier for this reaction is 0.16 eV. This result suggests that the dissociation process is feasible. Our structural optimization calculations predicted double O–H dissociated structures to be unstable; therefore, a barrier for that reaction is not well-defined. In summary, these results suggest faster reaction kinetics of $B(OH)_3$ dissociation on $NiO(001)$.

In the case of $B(OH)_3$ on $ZrO_2(\bar{1}11)$, we find that dissociative adsorption dominates and the boric acid molecule dissociates as it approaches the substrate. The potential energy diagram is shown in Figure 8. We consider two pathways starting from the most stable single O–H dissociated structure (1a). First, the single O–H dissociated structure can further dissociate in three possible ways, leading to double O–H dissociated bidentate structures (2a, 2b, and 2c). Second, the single O–H dissociated structure can transform into a cis-molecular adsorption configuration (3). The reaction pathway to form the most stable trans-molecular adsorption configuration required a rotation of the $B(OH)_3$ molecule on the surface by an angle of about 120° and is found to be kinetically improbable. Hence, it is believed to form via a separate independent attachment event.

Considering the first pathway, in order to form the double O–H dissociated structures, the H atom has to dissociate and hop onto different surface O atoms. The reaction energy barriers are 0.40, 0.44, and 0.74 eV for the pathways $1a \rightarrow 2a$, $1a \rightarrow 2b$, and $1a \rightarrow 2c$, respectively. In addition, we note that these double O–H dissociated structures are comparably favorable to the single O–H dissociated structure based on the

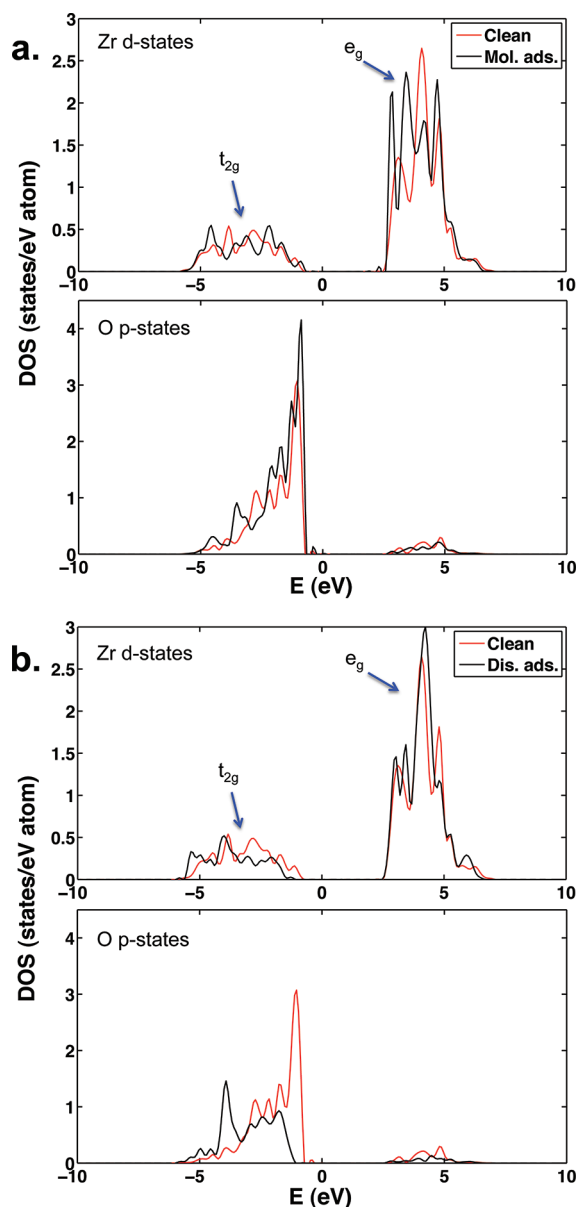


Figure 6. Projected density of states (PDOS) for the surface Zr and O atoms, obtained in the case of the most stable molecular adsorption (a) and dissociative adsorption (b). The states for the clean and adatom sites are marked in red and black, respectively.

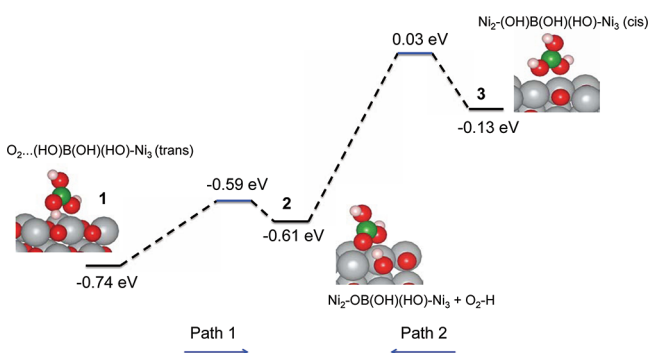


Figure 7. Potential energy diagram showing the reaction energy barriers for single O–H dissociation of $B(OH)_3$ on $NiO(001)$, starting from the trans-molecular configuration (Path 1) and cis-molecular configuration (Path 2).

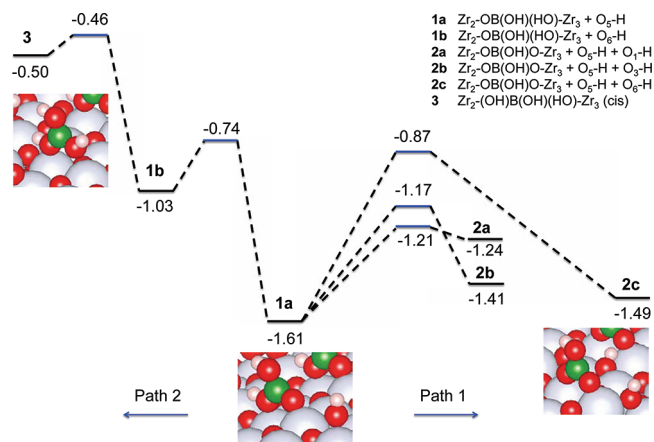


Figure 8. Potential energy diagram of $B(OH)_3$ on $ZrO_2(\bar{1}11)$ showing the energy barriers for two reaction pathways, further dissociation of the single O–H dissociated structure into double O–H dissociated structures (Path 1), and transition from a single O–H dissociated structure to a cis-molecular adsorption configuration (Path 2).

adsorption energy values. To assess the reaction rates, we choose the pathway between the single O–H dissociated state (1a) and the most stable double O–H dissociated state (2c), with an activation barrier of 0.74 eV. On the basis of our calculations, we find that the reaction rates between these two states are about 8–10 orders of magnitude lower compared with dissociation rates on $NiO(001)$, at a temperature of 300 K. Thus, we expect slow dissociation kinetics in the case of $B(OH)_3$ on $ZrO_2(\bar{1}11)$ at ambient temperatures. However, at higher operating temperatures in nuclear reactors, this reaction rate can increase significantly by about 6 orders of magnitude at 600 K. We now turn our attention to the second pathway, that is, the formation of the cis-molecular configuration. This pathway proceeds via an intermediate step, resulting in the formation of a metastable single O–H dissociated structure (1b). This intermediate structure occurs due to the hopping of a H atom from one O atom to another. The energy barrier for such a hopping event is found to be 0.89 eV. An additional 0.57 eV energy barrier has to be overcome in order to transition to the cis-molecular configuration. Thus, this pathway seems to be highly unlikely, and the single O–H dissociated structure will prevail. In summary, these results suggest slower reaction kinetics of $B(OH)_3$ dissociation on $ZrO_2(\bar{1}11)$.

From our results obtained here, we discuss possible design strategies to prevent boron and corrosion product deposition on fuel rods. Doping metal oxides at the nuclear fuel rod surfaces can be a possible design direction. In this regard, performing a systematic study of the surface reactivity with different dopants and developing reactivity descriptors (based on PDOS, such as the *d*-band model³⁸ and others³⁹) could help screen large number of candidates and find the least-reactive doped oxide. Activation barriers found in this study can be used as input parameters in higher-scale continuum models, and a quantitative description of boron deposition can be carried out.⁴⁰

CONCLUSIONS

The adsorption and dissociation of boric acid was studied on $NiO(001)$ and monoclinic $ZrO_2(\bar{1}11)$ surfaces for a coverage of 25% to understand the surface reactivity toward boric acid and the significance of these oxides in trapping boron in nuclear

reactors. Molecular adsorption of boric acid was found to be favorable on the NiO(001) surface, whereas dissociative adsorption was observed to be favorable on ZrO₂($\bar{1}11$). The most stable configuration for B(OH)₃ on NiO(001) is a hydrogen-bonded molecular structure, Ni_s-(OH)B(OH)-(OH)⋯O_s, with an adsorption energy of -0.74 eV. On ZrO₂($\bar{1}11$), a single O-H dissociated structure, Zr_s-(O)B(OH)(HO)-Zr_s + O_s-H, with an adsorption energy of -1.61 eV, is the most stable configuration. A study of the kinetics of these surface reactions showed high dissociation reaction rates on NiO(001) even at moderate temperatures, whereas low dissociation reaction rates on ZrO₂($\bar{1}11$) at moderate temperatures, which become significant only at high temperatures prevalent in nuclear reactor environments. The more exothermic adsorption of boric acid on the ZrO₂($\bar{1}11$) surface is in agreement with the results obtained from experiments,¹⁴ qualitatively. This predicts the significance of ZrO₂ in trapping boron in nuclear reactors. An analysis of the PDOS reveals higher surface reactivity of the ZrO₂($\bar{1}11$) surface over NiO(001) and highlights the fact that surface oxygen states play an important role along with the *d* states of the transition-metal atom in determining adsorbate-adsorbent interactions on metal oxide surfaces. Furthermore, we believe that the insights obtained here will be useful in the design of metal oxide catalytic systems and novel fuel rod materials and provide guidance in controlling the coolant chemistry for nuclear reactor applications.

■ ASSOCIATED CONTENT

● Supporting Information

Calculated bulk properties of NiO and ZrO₂, tilting of B(OH)₃ on the NiO(001) surface, and additional adsorption configurations of B(OH)₃ on the ZrO₂($\bar{1}11$) surface. This material is available free of charge via the Internet at <http://pubs.acs.org>.

■ AUTHOR INFORMATION

Corresponding Author

*E-mail: byildiz@mit.edu (B.Y.), jcg@mit.edu (J.C.G.).

Notes

The authors declare no competing financial interest.

■ ACKNOWLEDGMENTS

The authors acknowledge the financial support from the Consortium for Advanced Simulation of Light Water Reactors, an Energy Innovation Hub for Modeling and Simulation of Nuclear Reactors, under the U.S. Department of Energy Contract No. DE-AC05-00OR22725.

■ REFERENCES

- (1) Henrich, V. E.; Cox, P. A. *The Surface Science of Metal Oxides*; Cambridge University Press: Cambridge, U.K., 1994.
- (2) Yamaguchi, T. *Catal. Today* **1994**, *20*, 199–218.
- (3) Hannink, R. H. J.; Kelly, P. M.; Muddle, B. C. *J. Am. Ceram. Soc.* **2000**, *83*, 461–487.
- (4) Janney, M. A.; Calhoun, C. L.; Kimrey, H. D. *J. Am. Ceram. Soc.* **1992**, *75*, 341–346.
- (5) Schiller, G.; Henne, R.; Borck, V. J. *Therm. Spray Technol.* **1995**, *4*, 185–194.
- (6) Reissner, R.; Schulze, M. *Surf. Sci.* **2000**, *454–456*, 183–190.
- (7) Brailsford, A.; Yussouff, M.; Logothetis, E. *Sens. Actuators, B* **1997**, *44*, 321–326.
- (8) Raghunath, P.; Lin, M. C. *J. Phys. Chem. C* **2008**, *112*, 8276–8287.
- (9) Raghunath, P.; Lin, M. C. *J. Phys. Chem. C* **2009**, *113*, 3751–3762.
- (10) Peak, D.; Luther, G. W., III; Sparks, D. L. *Geochim. Cosmochim. Acta* **2003**, *67*, 2551–2560.
- (11) Deshon, J. EPRI Report 1008012; EPRI: Palo Alto, CA, 2004a.
- (12) Henshaw, J.; McGurk, J. C.; Sims, H. E.; Tuson, A.; Dickinson, S.; Deshon, J. *J. Nucl. Mater.* **2006**, *353*, 1–11.
- (13) Deshon, J. EPRI Report 1009734; EPRI: Palo Alto, CA, 2004b.
- (14) Deshon, J.; Frattini, P. EPRI Report 1003384; EPRI: Palo Alto, CA, 2002.
- (15) Decossin, E.; Fruzzetti, K. EPRI Report 1013681; EPRI: Palo Alto, CA, 2006.
- (16) Hawkes, J. M. Ph.D. Thesis, Georgia Institute of Technology, Atlanta, GA, 2004.
- (17) ul Haq, I.; Cinosi, N.; Bluck, M.; Hewitt, G.; Walker, S. *Nucl. Eng. Des.* **2011**, *241*, 155–162.
- (18) Sawicki, J. A. *J. Nucl. Mater.* **2008**, *374*, 248–269.
- (19) Wang, W.-D.; Wu, N. J.; Thiel, P. A. *J. Chem. Phys.* **1990**, *92*, 2025–2035.
- (20) Cappus, D.; Xu, C.; Ehrlich, D.; Dillmann, B.; Ventrice, C. A., Jr.; Al Shamery, K.; Kuhlenbeck, H.; Freund, H.-J. *Chem. Phys.* **1993**, *177*, 533–546.
- (21) Kitakatsu, N.; Maurice, V.; Hinnen, C.; Marcus, P. *Surf. Sci.* **1998**, *407*, 36–58.
- (22) Ignatchenko, A.; Nealon, D. G.; Dushane, R.; Humphries, K. J. *Mol. Catal. A: Chem.* **2006**, *256*, 57–74.
- (23) Ignatchenko, A. V. *J. Phys. Chem. C* **2011**, *115*, 16012–16018.
- (24) Korhonen, S. T.; Calatayud, M.; Krause, A. O. I. *J. Phys. Chem. C* **2008**, *112*, 6469–6476.
- (25) Kresse, G.; Furthmüller, J. *Phys. Rev. B* **1996**, *54*, 11169–11186.
- (26) Rohrbach, A.; Hafner, J.; Kresse, G. *Phys. Rev. B* **2004**, *69*, 075413.
- (27) Dudarev, S. L.; Botton, G. A.; Savrasov, S. Y.; Humphreys, C. J.; Sutton, A. P. *Phys. Rev. B* **1998**, *57*, 1505–1509.
- (28) Blöchl, P. E. *Phys. Rev. B* **1994**, *50*, 17953–17979.
- (29) Kresse, G.; Joubert, D. *Phys. Rev. B* **1999**, *59*, 1758–1775.
- (30) Perdew, J. P.; Chevary, J. A.; Vosko, S. H.; Jackson, K. A.; Pederson, M. R.; Singh, D. J.; Fiolhais, C. *Phys. Rev. B* **1992**, *46*, 6671–6687.
- (31) Vosko, S. H.; Wilk, L.; Nusair, M. *Can. J. Phys.* **1980**, *58*, 1200.
- (32) Methfessel, M.; Paxton, A. T. *Phys. Rev. B* **1989**, *40*, 3616–3621.
- (33) Blöchl, P. E.; Jepsen, O.; Andersen, O. K. *Phys. Rev. B* **1994**, *49*, 16223–16233.
- (34) Monkhorst, H. J.; Pack, J. D. *Phys. Rev. B* **1976**, *13*, 5188–5192.
- (35) Christensen, A.; Carter, E. A. *Phys. Rev. B* **1998**, *58*, 8050–8064.
- (36) Tian, S. X.; Xu, K. Z.; Huang, M. B.; Chen, X. J.; Yang, J. L.; Jia, C. C. *J. Mol. Struct.: THEOCHEM* **1999**, *469*, 223–227.
- (37) Zachariasen, W. H. *Acta Crystallogr.* **1954**, *7*, 305–310.
- (38) Hammer, B.; Norskov, J. K. *Adv. Catal.* **2000**, *45*, 71–129.
- (39) Vojvodic, A.; Hellman, A.; Ruberto, C.; Lundqvist, B. I. *Phys. Rev. Lett.* **2009**, *103*, 146103.
- (40) Deshon, J.; Hussey, D.; Kendrick, B.; McGurk, J.; Secker, J.; Short, M. *JOMMER* **2011**, *63*, 64–72.